ELSEVIER

Journal of Nuclear Materials 282 (2000) 89–96

journal of nuclear materials

www.elsevier.nl/locate/jnucmat

The surface rate constants of deuterium in the reduced activating martensitic steel OPTIFER-IVb

G.A. Esteban *, A. Perujo, L.A. Sedano [1], B. Mancinelli

European Commission, Joint Research Center, Environment Institute, T.P. 680, 21020 Ispra (VA), Italy

Received 20 July 2000; accepted 7 October 2000

Abstract

A gas permeation technique has been used to obtain the deuterium surface rate constants for adsorption σK_1 and recombination σK_2 in the martensitic steel OPTIFER-IVb. The measurements were performed over the temperature range 523–723 K with deuterium driving pressures ranging from 5×10^2 to 5×10^5 Pa. The deuterium surface rate constants obtained are: σK_1 (mol m^{-2} s^{-1} Pa^{-1}) $= 2.998 \times 10^{-8} \exp(-29230/RT)$, σK_2 (mol^{-1} m^4 s^{-1}) $= 2.838 \times 10^{-7} \exp(-28679/RT)$, R in J/K mol^{-1}. An intermediate gas transport regime has been accounted for over the experimental range. The transport regime was found close to the surface-limited regime as the deuterium driving pressure is lowered and the temperature increased. Permeability Φ has been derived together with surface rate constants: Φ (mol m^{-1} Pa$^{-1/2}$ s^{-1}) $= 5.311 \times 10^{-8} \exp(-44988/RT)$. This is in very good agreement with the permeability previously measured using a different gas evolution method, evidencing the consistency of the obtained results.

1. Introduction

Ferritic–martensitic steels are suitable blanket structural materials for thermonuclear fusion devices due to better swelling resistance, lower sensitivity to helium embrittlement and other thermophysical properties [1,2].

A series of reduced activating CrWVTa martensitic steels (OPTIFER) have been developed as a potential material for the blanket structures of a future fusion reactor [3,4]. Until recently the martensitic steel DIN 1.4914 (MANET) had been considered as the reference structural material for the design of a demonstration reactor (DEMO). In comparison to MANET, the new group of OPTIFER steels exhibits better activation properties, since alloying elements producing long-lived activation products have been substituted or eliminated. Amongst the whole series, OPTIFER-IVb has turned out to have quite an appropriate set of mechanical properties, showing a good balance between high fracture toughness, a low ductile-to-brittle transition temperature (DBTT) and a high creep strength.

Such a promising structural material needs a complete knowledge of its hydrogen (H) isotopes transport parameters in order to evaluate the recycling of H isotopes to the vacuum chamber, the retention of tritium within the blanket structures and the tritium permeation to cooling circuits. The H isotopes diffusive transport parameters of OPTIFER-IVb were evaluated in a previous work [5]. However, the understanding of H isotopes transport through the blanket structural materials of fusion reactors at low partial pressures ($<10^4$ Pa [6]) requires one to consider not only bulk properties, but also features related to the surface properties of the material. Moreover, as partial pressures are lowered the surface processes increasingly influence the kinetics and ultimately determine the rates of transport; especially, if oxides or other impurities are present on the material surface. The present work is aimed at obtaining the deuterium surface rate constants for adsorption σK_1 and recombination σK_2 in OPTIFER-IVb. These surface rate constants, together with those characterising the

* Corresponding author. Tel.: +39-0332 789 241; fax: +39-0332 785 029.

E-mail address: gustavo.esteban@jrc.it (G.A. Esteban).

[1] Present address: UPV-EHU, ETSIIT, Nuclear Engineering and Fluid Mechanics Department, 48013 Bilbao, Spain.

0022-3115/00/$ - see front matter
PII: S0022-3115(00)00485-2

diffusive transport [5], provide the necessary information to evaluate, by means of known numerical codes [7–10], the tritium permeation and retention.

2. Experimental

The material studied is OPTIFER-IVb [3,4]; a reduced-activating martensitic (RAM) 8% CrWVTa steel, heat number 986635, produced by Saarstahl GmbH (Germany). The specimen consisted of a thin disc with 0.8 mm thickness and 22 mm diameter, machined from a rod of material supplied by Forschungszentrum Kalsruhe. This physical configuration of the specimen emphasises surface effects, because large surface areas are available for surface reactions in comparison with a short diffusive length. In addition, it makes feasible the deuterium transport study using an infinite-slab (1-d) geometry approximation.

The chemical composition (wt%) is given in Table 1. It can be noticed that the elements producing long-lived activation products present in MANET such as Mo, Nb and Ni are absent. The stabilising grain size alloying element Nb has been substituted by Ta, whereas Mo has been substituted by W and Ni has been completely eliminated.

After machining, the specimens of steel underwent the normalising heat treatment that has demonstrated conferring the most appropriate set of mechanical properties [3]: austenising at 1223 K for 0.5 h, fast cooling, tempering at 1003 K for 3 h and finally slow cooling to room temperature. This heat treatment guarantees a fine pre-austenitic grain size, a fully martensitic phase and no pre-eutectoid carbide precipitation.

The surface of the specimen was mechanically polished and degreased before insertion into the experimental rig, thus only oxide layers resulting from exposure to air at room temperature should be present.

Table 1
Chemical composition of OPTIFER-IVb and MANET-II (wt%)

	OPTIFER-IVb	MANET-II
C	0.12	0.11
Cr	8.3	10.3
Nb	–	0.14
Ta	0.06	–
Mo	–	0.58
W	1.4	–
Ni	–	0.65
Mn	0.34	0.85
V	0.22	0.19
N	0.03	0.03
Fe	Balance	Balance

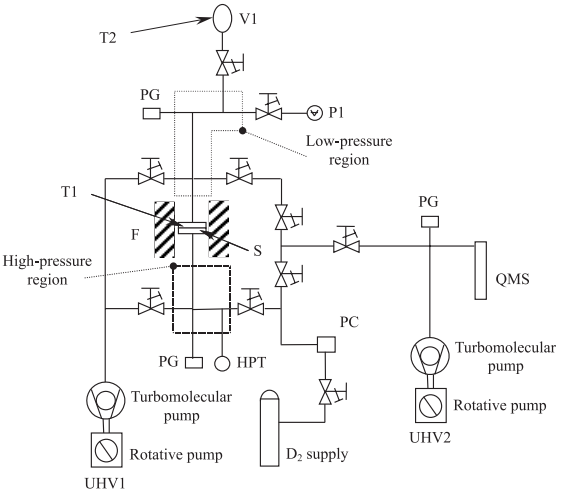

Fig. 1. Schematic view of the permeation facility. PG: penning gauge; F: furnace; PC: pressure controller; HPT: high-pressure transducer; QMS: quadrupole mass spectrometer; S: specimen; T1, T2: nickel/chromium–nickel thermocouples; P1: capacitance manometer; UHV: ultra high vacuum pumping units; V1: calibrated volume.

A schematic view of the installation used is shown in Fig. 1. This installation and the procedure for a measurement have been described in earlier works [11–13]. Here we will briefly describe them for completeness. The rig comprises standard ultra high vacuum (UHV) stainless steel components. The UHV is needed before any measurement is obtained by two pumping units (UHV1 and UHV2); both of them comprise a turbomolecular and a two-stage rotary pump. A good level of vacuum, about 10^{-6} Pa, is reached prior to system bakeout, and about 10^{-7} Pa, afterwards. Several penning gauges (PG) together with a quadrupole mass spectrometer (QMS) control the quality of the vacuum reached.

The specimen (S) is placed between two flanges set into a resistance furnace allowing measurements at an experimental temperature of 723 K and lower. A nickel/chromium–nickel thermocouple (T1) held in a well (drilled into one of the flanges) permits temperature control with a stability of ± 1 K. Two gold O-rings ensure the leak tightness of the specimen.

A single run of the experiment consists of holding one surface of the specimen at a certain high gas pressure level; forcing its permeation through the specimen to the low-pressure region (Fig. 1). The desired driving pressure is controlled by a high-pressure transducer (HPT) and a pressure controller (PC), whereas a capacitance manometer (P1) with a full scale reading of 100 Pa measures the pressure increase due to permeation through the sample. The low-pressure volume is calibrated in every test to allow a direct conversion of the

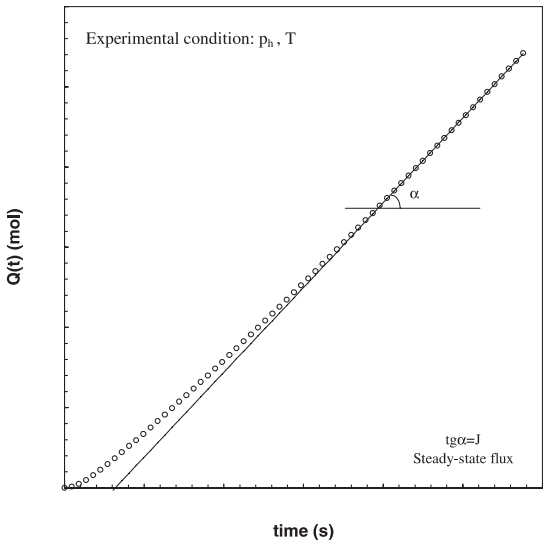

Fig. 2. Characteristic permeation curve. ○ deuterium permeated quantity; – deuterium permeated quantity in the steady state. $Q(t)$: total amount of gas permeated from the high to the low pressure region.

pressure level into the amount of permeated gas $Q(t)$. Likewise, the pressure increase rate may be converted into the amount of gas permeated per specimen unit area and time (gas flux, $J(t) = \partial Q(t)/\partial t$). The modelling of the pressure increase $p(t)$, due to the gas permeation in the low-pressure region, makes it possible to derive the transport parameters in the diffusion or surface-limited transport regimes. A characteristic permeation curve is depicted in Fig. 2.

3. Theory

In many cases it has been experimentally proved and theoretically studied [14–19] that under certain conditions (i.e., low pressure level, oxidised or contaminated surfaces) the H isotopes transport regime becomes surface limited, i.e., H transport within the material is governed by the physico-chemical reactions (adsorption, dissociation, recombination, desorption) occurring at the surface of the material, rather than diffusion limited, where H transport is limited by the diffusion of H atoms through the host matrix of the bulk of the material.

The evaluation of such processes leads one to consider an adsorption flux and a recombination flux through the surface of the studied material. The net H flux entering the material J, can be expressed as

$$J = \sigma K_1 p - \sigma K_2 c^2, \tag{1}$$

K_1 and K_2 being the adsorption and recombination rate constants, respectively. σ is the surface roughness expressing the quotient between the real and the geometrical areas of the surface, p (Pa) the H driving pressure and c (mol m^{-3}) is the H concentration at the subsurface of the material.

If the whole specimen of material is exposed to a certain partial pressure of H, p, for enough time to reach a saturation state, an equilibrium concentration in the bulk, the same as the H subsurface concentration, c_{eq}, is reached. Thus, recombinative and adsorptive fluxes show dynamic equilibrium cancelling each other:

$$0 = \sigma K_1 p - \sigma K_2 c_{eq}^2. \tag{2}$$

In the described equilibrium state Sieverts' law, $c_{eq} = K_s p^{1/2}$, is fulfilled. Hence, a direct relationship between surface rate constants, K_1, K_2 and Sieverts' constant, K_s, arises:

$$K_s = \sqrt{\frac{K_1}{K_2}}. \tag{3}$$

It is worth noting that, once the Sieverts' constant is known and using the previous expression (3), it is only necessary to evaluate one of the surface rate constants in order to define completely the surface-limited H transport. Furthermore, the most reliable attempts in theoretically defining the surface-limited transport regime, the Baskes model [16] and the Pick and Sonnenberg model [17], allow the calculation of the adsorption constant K_1 rather than K_2, since K_1 can be easily evaluated in terms of a simple kinetic theory. The conclusions reached in those works propose the following expressions for the adsorption constant.

For Baskes' approximation [16],

$$K_1 = \frac{2Cs\sigma}{(2mT)^{1/2}} \exp\left(\frac{-E_x}{RT}\right),$$
$$(E_x = \max(0, E_s + E_d)). \tag{4}$$

For Pick and Sonnenberg's approximation [17]:

$$K_1 = \frac{Cs\sigma}{(2mT)^{1/2}}, \tag{5}$$

where C is a kinetic constant equal to 4.376 mol K$^{1/2}$ u$^{1/2}$ Pa^{-1} m^{-2} s^{-1}. s is the 'sticking coefficient' expressing the probability that a H atom remains 'stuck' to an adsorption surface site; it is activated with an energy of $2E_C$ because both the two atoms from the H_2 molecule must surpass the sticking barrier E_C:

$$s = s_0 \exp\left(\frac{-2E_C}{RT}\right), \tag{6}$$

where m is the H isotope atomic mass (a.m.u.), T the temperature (K) and R is the ideal gas constant (8.314 J K^{-1} mol^{-1}). The differences between both models have been discussed in [18].

The theoretical model used here to study the permeation experiment analyses an intermediate transport regime, i.e., hydrogen transport kinetics is not exclusively limited either by diffusion within the bulk of the material or by surface reactions, but a combination of both of them [12]. In this manner the permeability Φ (mol m^{-1} Pa$^{-1/2}$ s^{-1}) can be evaluated together with the surface rate constants K_1 and K_2, by analysing the relationship of steady-state permeation fluxes with gas driving pressures over the experimental temperature range. The general equation of steady-state permeation through an infinite symmetric slab in an intermediate regime has been developed in [20]; here, we will briefly explain it for completeness.

In Fig. 3, all the involved H fluxes are represented, either those coming from surface reaction processes, recombination $J_{o,h} = \sigma_h K_{2,h} c_h^2$, $J_{o,l} = \sigma_l K_{2,l} c_l^2$, and adsorption $J_{i,h} = \sigma_h K_{1,h} p_h$, $J_{i,l} = \sigma_l K_{1,l} p_h$, or the diffusive flux $J_d = -D(\partial c(x)/\partial x)$. The subscripts indicate 'o' out, 'i' in, 'l' low-pressure region, 'h' high-pressure region, 'd' diffusive. It is worth noting that only the steady-state permeation is accounted for at this stage; that is why a linear profile of concentration is built up within the bulk of material. Such a profile remains invariable during the steady-state permeation so that no H inventory accumulation or diminution is produced.

The following hypotheses are assumed:

- Symmetric slab: $\sigma_h K_{1,h} = \sigma_l K_{1,l} = \sigma K_1$, $\sigma_h K_{2,h} = \sigma_l K_{2,l} = \sigma K_2$.
- Low pressure side simplification: $p_h \gg p_l \approx 0$, $J_{i,l} = \sigma K_1 p_l = 0$.

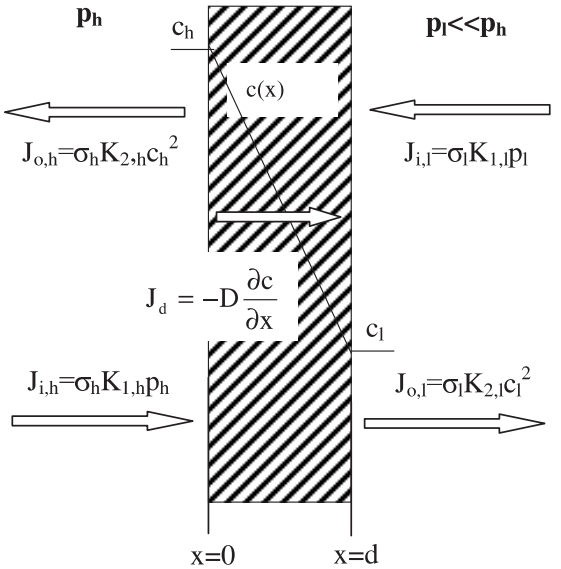

Fig. 3. Scheme of the permeation process through an infinite-slab (permeation is assumed to proceed exclusively in the transversal direction). Intermediate transport regime.

Some new parameters are defined to simplify the mathematical study:

- The 'reduced concentration': $C(x) = c(x)/c_{eq}$; being $c_{eq} = K_s p_h^{1/2}$ the equilibrium H concentration reached if the entire specimen (i.e., both sides of it) is exposed to the pressure p_h.
- The 'permeation number':

$$W = \frac{\sigma K_1 p_h}{(\Phi/d)\sqrt{p_h}} = \frac{\sigma K_1 d}{\Phi}\sqrt{p_h},$$

is the quotient of the adsorption flux at $x = 0$ (high-pressure side) and the steady-state flux in a pure diffusive regime. W states the gas transport regime; i.e., whether the regime is pure diffusion-limited ($W \gg 1$), pure surface-limited ($W \ll 1$), or an intermediate one between both of them.

Considering the H mass balance at the surface facing the low-pressure region, $x = d$ (Fig. 3):

$$J_d = J_{o,l} - J_{i,l} \approx J_{o,l} = J \tag{7}$$

and at the surface facing the high-pressure region, $x = 0$:

$$J_{i,h} - J_{o,h} = J_d \tag{8}$$

and taking into account the linear profile of H concentration for the diffusive flux definition, $J_d = -D(\partial c/\partial t) = D(c_h - c_l)/d$, the general equation for the steady-state permeation through a symmetric membrane is easily derived in terms of the permeation number W and the reduced concentration at the subsurface of the low-pressure region C_l:

$$W^2 C_l^4 + 2W C_l^3 + 2C_l^2 = 1. \tag{9}$$

This reduced concentration can be expressed in terms of the H fluxes as

$$C_l^2 = \frac{c_l^2}{c_{eq}^2} = \frac{\sigma K_2 c_l^2}{\sigma K_2 K_s^2 p_h} = \frac{J}{\sigma K_1 p_h} = \frac{J}{J_{i,h}}. \tag{10}$$

The general equation (9) establishes a relationship between this reduced concentration $C_l^2 = J/\sigma K_1 p_h$ and the permeation number $W = \sigma K_1 d\sqrt{p_h}/\Phi$, i.e., the directly measurable quotient J/p_h is a function of p_h through the unknown parameters σK_1 and Φ.

From the expression (9) it can be noticed that for low permeation numbers $W \ll 1$, the steady-state permeation equation becomes

$$2C_l^2 = 2\frac{J}{J_{i,h}} = 1, \tag{11}$$

$$J = \frac{1}{2}J_{i,h} = \frac{1}{2}\sigma K_1 p_h. \tag{12}$$

This is the steady-state permeation equation for a pure surface-limited regime. On the other hand, for high permeation numbers W $\gg$ 1 Eq. (9) becomes

$$C_1^2 = \frac{1}{W}, \tag{13}$$

that is,

$$\frac{\sigma K_2 c_1^2}{\sigma K_2 c_{eq}^2} = \frac{\Phi}{\sigma K_1 d p_h^{1/2}}, \tag{14}$$

which leads to

$$J = J_{o,1} = \frac{\Phi}{d} p_h^{1/2}. \tag{15}$$

This is the steady-state permeation equation for a pure diffusion limited regime. The solution of the general equation (9) has been evaluated numerically [12]:

$$\log\left(C_1^2\right) = \frac{\sum_{n=0}^{5} a_n (\ln W^2)^n}{\sum_{n=0}^{5} b_n (\ln W^2)^n} \tag{16}$$

with $a_0 = -0.5314$, $a_1 = -0.0927$, $a_2 = -0.01828$, $a_3 = -0.00126$, $a_4 = -5.4621 \times 10^{-5}$, $a_5 = -8.201 \times 10^{-7}$, $b_0 = 1$, $b_1 = 0.011$, $b_2 = 0.011295$, $b_3 = 1.7448 \times 10^{-5}$, $b_4 = 8.9754 \times 10^{-6}$, $b_5 = -4.666 \times 10^{-8}$.

Fig. 4 depicts this function showing how the extremes approach pure surface or diffusion limited regimes; it can be re-written in terms of the directly measurable data $\{J/p_h\}, p_h\}$ and the unknown parameters σK_1 and Φ as

$$\log\left(\frac{J}{p_h}\right) = \log(\sigma K_1) + \frac{\sum_{n=0}^{5} a_n \left(\ln\left((\sigma K_1 d/\Phi)^2 p_h\right)\right)^n}{\sum_{n=0}^{5} b_n \left(\ln\left((\sigma K_1 d/\Phi)^2 p_h\right)\right)^n}. \tag{17}$$

4. Results and discussion

A series of permeation runs have been performed within the temperature range of 523–723 K with deuterium driving pressures, p_h, ranging from 5×10^2 to 5×10^5 Pa.

In Fig. 5 the obtained steady-state permeation fluxes for different temperatures are depicted versus the driving pressure. It can be noticed that the permeation regime does not correspond to a well-defined diffusion (Eq. (15)) or surface-limited (Eq. (12)) permeation regime; because steady-state permeation fluxes follow a proportional law with a power of the driving pressure ranging from 0.90 to 0.66, i.e., it deviates from the limits 0.5 or 1. Thereby an intermediate permeation regime is evidenced. Nevertheless, it can be observed that the lower the driving pressure applied the closer the transport regime gets to a surface-limited type, i.e., the exponent of the driving pressure approximates to 1.

In each permeation run, the 'permeation flux'-to-'driving pressure' quotient, J/p_h, is obtained for each pressure p_h and temperature T. A non-linear least-squares fitting routine fits the experimental points $\{(J/p_h), p_h\}$ with the theoretical function (17) for each temperature, σK_1 and Φ being the fitting parameters. Fig. 6 shows a good agreement between experimentally obtained results and the resultant fitting curves. The values of σK_2 are derived from the σK_1 ones by means of Eq. (3) with the deuterium Sieverts' constant in OPTIFER-IVb defined in [5].

Subsequently, a linear least-squares fitting routine fits the groups of previously obtained $\sigma K_1, \sigma K_2$ and Φ to an Arrhenius behaviour, extracting the pre-exponentials

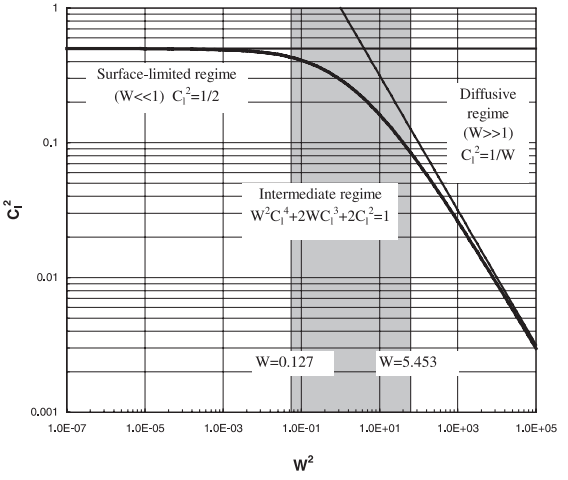

Fig. 4. Graphic solution of the general equation for the steady-state permeation. W: permeation number, C_1: reduced concentration at the subsurface of the low-pressure region. Experimental range measured for the permeation number W: ▭.

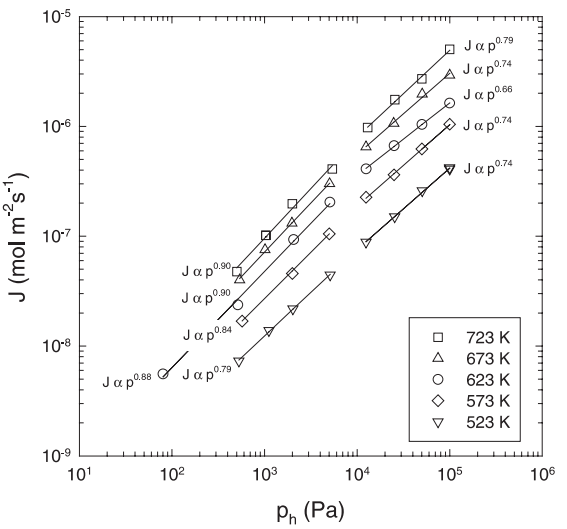

Fig. 5. Steady-state permeation fluxes, J, versus gas driving pressures, p_h: transport regime characterisation.

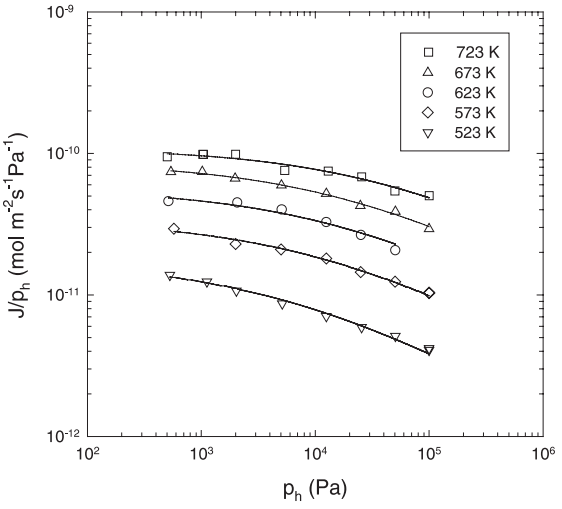

Fig. 6. Fitting curves for permeation experimental results.

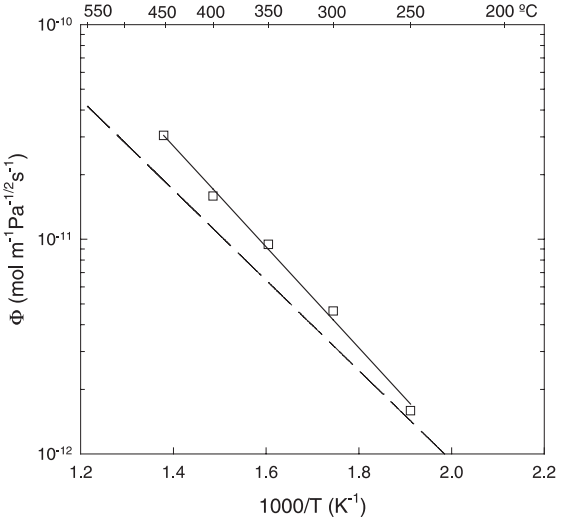

Fig. 7. Arrhenius plot of the permeabilities. The solid line refers to this work, the dashed line to isovolumetric desorption experiment [5].

$\sigma K_{01}, \sigma K_{02}, \Phi_0$ and the activation energies for adsorption, E_1, recombination, E_2 and permeation, E_p.

The obtained permeability agrees (10% of deviation in E_p) with the value measured by means of the isovolumetric desorption technique for the interaction of OPTIFER-IVb with deuterium [5] (Fig. 7). The permeability obtained here is

$$\Phi\ (\mathrm{mol\ m^{-1}\ Pa^{-1/2}\ s^{-1}}) = 5.311 \times 10^{-8} \exp(-44988/RT).$$

The obtained surface rate constants are

$$\sigma K_1(\mathrm{mol\ m^{-2}\ s^{-1}\ Pa^{-1}}) = 2.998 \times 10^{-8} \exp(-29230/RT),$$

$$\sigma K_2(\mathrm{mol^{-1}\ m^4\ s^{-1}}) = 2.838 \times 10^{-7} \exp(28679/RT).$$

The permeation number W has been evaluated for each permeation run (Table 2). It is a remarkable fact that all the permeation numbers range from 0.127 to 5.453; these values cannot be considered either $W \gg 1$ or $W \ll 1$, noticing that an intermediate transport regime effectively occurs, rather than a pure diffusion-limited or a pure surface-limited regime (Fig. 4). From Table 2 it is evidenced that the permeation number diminishes as the driving pressure is lowered and the experimental temperature increases. As a consequence, the surface effects for OPTIFER-IVb become more important in deuterium transport characterisation not only when the deuterium experimental pressure level is lower, but, simultaneously, when the experimental temperature is higher. Moreover, we have evaluated an activation energy for the permeation number equalling $(E_1 - E_p) = -15758\ \mathrm{J\ mol^{-1}}$.

The Arrhenius plot of the obtained surface rate constants is compared with other works in Figs. 8 and 9. The values for σK_1 and σK_2 obtained here are close to those of MANET in [11]. The Baskes and the Pick and Sonnenberg models have been applied (Eqs. (3)–(5)) for OPTIFER-IVb with the diffusive transport parameters from [5]; they yielded the following values of the activation energy of the recombination constant, K_2: $-57910\ \mathrm{J\ mol^{-1}}$ (Pick and Sonnenberg), $-17634\ \mathrm{J\ mol^{-1}}$ (Baskes). The difference between K_1 and K_2 values from

Table 2
Experimental permeation numbers (W)

p_h (Pa) \ T (K)	723	673	623	573	523
10^5	1.792	2.727	–	3.664	5.453
5×10^4	1.267	1.940	2.11	2.592	3.878
2.5×10^4	0.907	1.362	1.492	3.662	2.752
1.25×10^4	0.647	0.964	1.052	1.831	1.929
5×10^3	0.416	0.613	0.670	1.295	1.235
2×10^3	0.253	0.384	0.428	0.819	0.777
10^3	0.182	0.275	–	0.518	0.576
5×10^2	0.127	0.201	0.213	0.277	0.397

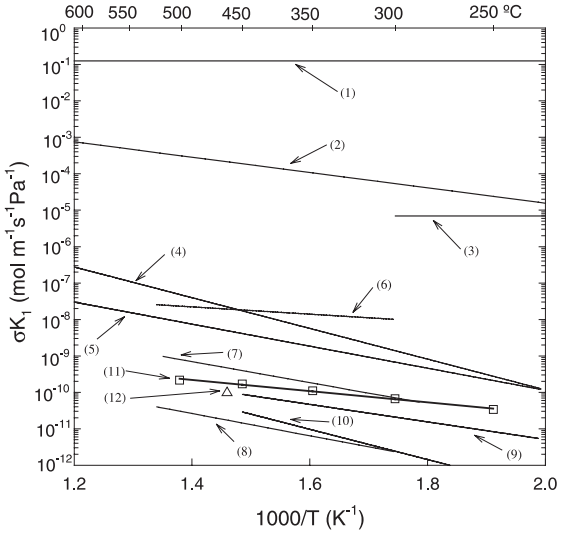

Fig. 8. Arrhenius plot of adsorption rate constants. (1) and (2) Pick and Sonnenberg [17] model and Baskes [16] model, respectively, for OPTIFER-IVb (with sticking coefficient $s = 1$ and roughness $\sigma = 1$); (3) D^+ implantation in MANET [21]; (4) H_2, 316 SS ion beam cleaned [22]; (5) H_2, 316 SS oxidized both surfaces [22]; (6) D_2, bare MANET [12]; (7) D_2, MANET [11]; (8) D_2, oxidized MANET [12]; (9) D_2, Inconel 600 [23]; (10) D_2, 304 SS [24], (11) D_2, OPTIFER-IVb (this work); (12) D_2, OPTIFER-IVb (isovolumetric desorption technique).

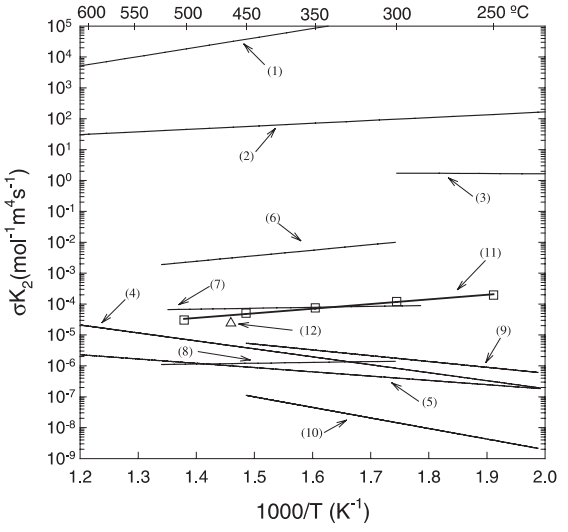

Fig. 9. Arrhenius plot of recombination rate constants. (1) and (2) Pick and Sonnenberg [17] model and Baskes [16] model, respectively, for OPTIFER-IVb (with sticking coefficient $s = 1$ and roughness $\sigma = 1$); (3) D^+ implantation in MANET [21]; (4) H_2, 316 SS ion beam cleaned [22]; (5) H_2, 316 SS oxidized both surfaces [22]; (6) D_2, bare MANET [12]; (7) D_2, MANET [11], (8) D_2, oxidized MANET [12]; (9) D_2, Inconel 600 [23]; (10) D_2; 304 SS [24]; (11) D_2, OPTIFER-IVb (this work); (12) D_2, OPTIFER-IVb (isovolumetric desorption technique).

these two models and the surface rate constants measured in this work can be explained assuming two values for the product of the effective roughness and sticking coefficient: $(\sigma \cdot s)_{PS} = 2.4 \times 10^{-7} \exp(-29230/RT)$ and $(\sigma \cdot s)_B = 3.0 \times 10^{-8} \exp(+11046/\ RT)$ for the Pick and Sonnenberg model and the Baskes model, respectively.

The isovolumetric desorption technique [5] was used to obtain the same deuterium surface rate constants for OPTIFER-IVb. In that case a progressive change in the surface state of the specimens due to oxidation did not allow verifying an Arrhenius behaviour for them. However, the first values found for the surface rate constants using this technique agreed well with the values represented here (see Figs. 8 and 9, one-triangled point depicted). The experience showed how surface oxidation is crucial for hydrogen transport definition, accentuating surface effect over diffusion and diminishing surface rate constant values.

5. Conclusions

A gas permeation technique has been used over a temperature range of 523–723 K and deuterium driving pressure ranging from 5×10^2 to 5×10^5 Pa to obtain the surface rate constants of deuterium, adsorption σK_1 and recombination σK_2, in the martensitic steel OPTIFER-IVb. An intermediate transport regime, neither pure surface-limited nor pure diffusion-limited, has been evidenced under the experimental conditions applied. The study of permeation in such a regime leads to a deuterium permeability in good agreement with previous results obtained by means of a different gas evolution technique. The analysis of the permeation number W proves that, besides the presence of impurities in the surface of the material and the reduction of the permeation path, both low pressures and high temperatures make surface effects in OPTIFER-IVb becoming more determinant when characterising deuterium transport.

References

[1] K.S. Forcey, I. Iordanova, M. Yaneva, J. Nucl. Mater. 240 (1997) 118.
[2] E. Serra, A. Perujo, G. Benamati, J. Nucl. Mater. 245 (1997) 108.
[3] L. Schäfer, M. Schirra, K. Ehrlich, J. Nucl. Mater. 233–237 (1996) 264.
[4] K. Ehrlich, S. Kelzenberg, H.-D. Röhrig, L. Schäfer, M. Schirra, J. Nucl. Mater. 212–215 (1994) 678.
[5] G.A. Esteban, A. Perujo, K. Douglas, L.A. Sedano, J. Nucl. Mater. 281 (2000) 34.
[6] F. Reiter, S. Tominetti, A. Perujo, Fus. Eng. Des. 15 (1992) 223.
[7] K.J. Dietz, F. Waelbroeck, P. Wienhold, Jül-1448, 1997.

[8] M.I. Baskes, SAND 83-8231, 1983.
[9] P. Wienhold, M. Profant, F. Waelbroeck, J. Winter, Jül-1825, 1983.
[10] G. Gervasini, F. Reiter, J. Nucl. Mater. 155–157 (1988) 754.
[11] E. Serra, A. Perujo, J. Nucl. Mater. 223 (1995) 157.
[12] E. Serra, A. Perujo, J. Nucl. Mater. 240 (1997) 215.
[13] E. Serra, A. Perujo, K.S. Forcey, Vuoto 3 (1997) 18.
[14] A. Perujo, K. Douglas, E. Serra, Fus. Eng. Des. 31 (1995) 101.
[15] P.M. Richards, J. Nucl. Mater. 152 (1988) 246.
[16] M.I. Baskes, J. Nucl. Mater. 92 (1980) 318.
[17] M.A. Pick, K. Sonnenberg, J. Nucl. Mater. 131 (1985) 208.
[18] P.M. Richards, J. Nucl. Mater. 152 (1988) 246.
[19] A.D. Le Claire, in: The Permeation of Gases Through Solids. I – Principles, AERE-R 9911, 1981.
[20] F. Waelbroeck, P Wienhold, J. Winter, E. Rota, T. Banno, Jül-1966.
[21] L.A. Sedano, A. Perujo, J. Camposilvan, G.B. Cueroni, K. Douglas, in: The deuterium recombination and dislocation constants in MANET derived from plasma implantation experiments, JRC Euroreport EUR 17713 EN (1997).
[22] D.M. Grant, D.L. Cummings, D.A. Blackburn, J. Nucl. Mater. 152 (1988) 139.
[23] E. Rota, F. Waelbroeck, P. Wienhold, J. Winter, J. Nucl. Mater. 111&112 (1982) 233.
[24] M. Braun, B. Emmoth, F. Waelbroeck, P. Wienhold, J. Nucl. Mater. 93&94 (1980) 861.